Analyst

PAPER

View Article Online
View Journal

Cite this: DOI: 10.1039/d6an00128a

Biochemical composition of prostate core-needle biopsies before and after a single fraction of 13.5 Gy: a Raman spectroscopy-based study

Kirsty Milligan,[a] Mitchell Wiebe,[a] Alejandra Fuentes,[a] Sandra Popescu,[a] Ramie Ali-Adeeb,[b] Jeffrey Andrews,[a] Julian Lum,[c,d] Alexandre Brolo,[b] Christina Haston,[a] Bibi Naghibi Torbati,[e] Juanita Crook[f] and Andrew Jirasek *[a]

High dose rate brachytherapy (HDR-BT) is an attractive option for patients with favourable-risk intermediate-grade prostate cancer. However the relationship between radiation dose and the biochemical response of tumours remains poorly understood. The aim of this study was to investigate the tissue composition of prostate core-needle biopsies, before and after a single dose (13.5 Gy) of HDR-BT using Raman Spectroscopy (RS) and Group and Basis Restricted Non-Negative Matrix Factorisation (GBR-NMF) modelling. RS was used to measure the spectral profiles of benign and malignant regions of prostate tissue. GBR-NMF was employed to derive biochemical profiles from Raman spectra of core-needle biopsies, encompassing both benign and malignant areas, from patients with intermediate risk prostate cancer (PCa). Thirty-four biochemicals were included in the RS evaluation of 40 biopsy samples from 20 patients. Eight biochemicals were significantly differentially expressed between pre- and post-HDR-BT benign tissue (13.5 Gy single fraction): citric acid, collagen, cysteine, DNA, glycerol, palmitic acid, tryptophan, and lycopene (by Mann–Whitney *U* test). The model identified phenylalanine, stearic acid and retinol to be differentially expressed in malignant tissue after a single dose of 13.5 Gy high dose rate brachytherapy. β-Carotene was found to differ in expression between benign and malignant prostate tissue, irrespective of radiation exposure. Carotenoids and phospholipids may influence the tumour microenvironment (TME) through several mechanisms that affect cancer progression and response to treatments like radiation therapy. These biochemical changes could identify potential therapeutic targets for a personalised radiation treatment approach.

Received 2nd February 2026,
Accepted 7th May 2026

DOI: 10.1039/d6an00128a

rsc.li/analyst

Introduction

Prostate cancer (PCa) is the most commonly diagnosed cancer among men in Canada and the Canadian Cancer Society estimates that 1 in 8 men will be diagnosed with prostate cancer in their lifetime.[1] Most prostate cancers are now diagnosed while clinically localised due to increased rates of prostate specific antigen (PSA) screening, however, both intermediate and high grade localised PCa will usually be treated with some form of radiation therapy (RT).[2–4]

High dose rate brachytherapy (HDR-BT) is an especially attractive option for patients with favourable-risk intermediate-grade prostate cancer. This technique delivers high doses of radiation directly to the prostate whilst sparing surrounding healthy tissues. Advances in hypo-fractionation and personalised treatment planning have further optimised clinical outcomes and control rates.[5] Despite these improvements, the relationship between radiation dose and the biochemical response of tumours remains poorly understood. Whilst higher doses are generally associated with improved local control, individual tumours often exhibit variable responses due to factors such as genetic heterogeneity and differences in the tumour microenvironment (TME).[6] Understanding how these factors influence treatment efficacy is critical for optimising radiation treatment plans. A deeper insight into the biochemical changes induced by HDR-BT could enable clinicians

[a]Department of Computer Science, Mathematics, Physics and Statistics, The University of British Columbia Okanagan Campus, Kelowna, Canada. E-mail: andrew.jirasek@ubc.ca
[b]Department of Chemistry, University of Victoria, British Columbia, Canada
[c]Trev and Joyce Deeley Research Centre, BC Cancer, Victoria, British Columbia, Canada
[d]Department of Biochemistry and Microbiology, University of Victoria, Victoria, Canada
[e]Department of Pathology and Laboratory Medicine, University of British Columbia, Kelowna, British Columbia, Canada
[f]Department of Radiation Oncology, University of British Columbia, Kelowna, British Columbia, Canada

to tailor treatment plans based on a patient's unique biochemical tumour profile, thereby improving outcomes and minimising side effects. This personalised approach to radiation therapy has the potential to enhance both therapeutic effectiveness and quality of life for patients with prostate cancer.

The TME plays a crucial role in determining the response of tumours to radiation therapy. The TME consists of a complex network of cancer cells, immune cells, stromal cells, blood vessels, extracellular matrix (ECM), and signalling molecules that collectively influence tumour growth,[6] progression,[7,8] and treatment outcomes.[9] Key components of the TME, such as hypoxia and immune suppression have been shown to significantly impact radiation response.[10,11]

Hypoxia is a hallmark of many tumours, including prostate cancer. Oxygen can behave as a radiosensitiser, in that that well-oxygenated tumour cells are more susceptible to radiation-induced DNA damage. In contrast, hypoxic regions within the tumour are often resistant to radiation because the lack of oxygen reduces the formation of reactive oxygen species (ROS), which are critical for effective DNA damage. Efforts to overcome hypoxia, such as using hypoxia-targeting agents or delivering higher doses of radiation to hypoxic areas, are ongoing but remain challenging.[12] Carotenoids, a class of natural pigments found in fruits and vegetables, are known for their antioxidant properties and potential implication in cancer prevention.[13–15] In the context of prostate cancer, carotenoids—especially lycopene, β-carotene, and lutein—may influence the TME through several mechanisms that affect cancer progression and response to treatments like radiation therapy. Carotenoids affect reactive oxygen species (ROS) and reduce oxidative stress, which can otherwise promote DNA damage, genetic instability, and cancer progression.[16,17] Since RT relies on ROS to induce DNA damage in cancer cells, the antioxidant effects of carotenoids could theoretically reduce radiation efficacy. However, a balance between antioxidant protection of normal tissues and selective sensitisation of cancer cells may be beneficial.[18]

Carotenoids have also been shown to display involvement in (i) inflammation and immune modulation by inhibiting the production of pro-inflammatory cytokines such as IL-6, TNF-α, and COX-2,[19,20] and (ii) inhibition of angiogenesis and therefore limited tumour growth[21,22] and androgen-receptor (AR) signalling, which helps to limit tumour progression.[22,23] Studies have shown that diets rich in carotenoids, particularly lycopene from tomatoes, are associated with a reduced risk of prostate cancer.[24,25] Carotenoids may enhance the effects of certain treatments by modulating the TME. However, carotenoid interaction with radiation therapy in prostate tissue is not well researched, and could have important implications in HDR-BT as their antioxidant properties could both protect normal tissues and potentially reduce treatment efficacy if not properly balanced.

Raman spectroscopy (RS) is a non-invasive, label-free detection technique, capable of monitoring biochemical changes at the molecular level.[26] By identifying unique vibrational fingerprints, RS can monitor carotenoids and dynamic profiles of other biomolecules such as lipids and proteins within cells and tissues. Owing to this, there have been numerous studies to date that have employed Raman spectroscopy as a method of cell and tissue characterisation.[27–34] As such, RS can provide insight into how carotenoids change in tissue post-RT and also how these antioxidant molecules interact with other biomolecules within tissue, potentially helping to assess treatment responses or resistance mechanisms in prostate cancer.

Herein, we investigate the biochemical composition of prostate core-needle biopsies, in particular carotenoid content, before and after a single dose (13.5 Gy) of HDR-BT using RS and GBR-NMF modelling.[27,35] The goals of this study are to: (i) assess the potential of Raman spectroscopy as a diagnostic tool in radiation therapy, and (ii) better understand the role of carotenoids and adjacent biochemicals in prostate cancer TME and HDR-BT response.

Methods

Patient cohort

The 20 patients included in this study received HDR-BT as mono-therapy for intermediate risk prostate adenocarcinoma. All individuals involved in this study provided informed consent for the use of bio-specimens and reporting of results for research purposes. All identifiable information has been omitted for each individual. All methods and procedures were carried out in accordance with the procedures and guidelines provided by Health Canada and Public Health Agency of Canada Research Ethics Board (REB# H17-02904). The study has been approved by the University of British Columbia and BC Cancer Research Ethics Boards. Prior multi-parametric MRI had identified the dominant lesion, the location of which was transferred to transrectal ultrasound (TRUS) images through rigid registration for the purpose of targeting the lesion for both biopsy and dose escalation. HDR BT dose prescription was 27 Gy in 2 fractions (*i.e.* 13 Gy per fraction ×2 fractions), given in 2 separate procedures 2 weeks apart. Biopsies were collected prior to both the first and second fractions. A biopsy was not collected post second fraction due to collection and standard of practice limitations. Dose escalation to the dominant lesions aimed for 140–150% of prescription, that is, the planned dose was up to 140–150% of the prescription in the main lesion, largely due to the high dose gradients present within brachytherapy treatment. Biopsies were taken under anaesthesia, transperineally with template and ultrasound guidance based on the prior fusion, prior to the first treatment and 2 weeks later of the same area, prior to the second treatment. Samples were immediately placed in hypothermosol. Paired samples were sent for haematoxylin and eosin (H&E) staining and examination at KGH pathology to confirm tumour presence and accurate targeting. The 20 patients were assigned patient numbers (shown in Table 2). A single pre-treatment and a single post-treatment biopsy was obtained from each individual (40 biopsies in total). All

patients had been diagnosed with intermediate stage prostate cancer prior to the commencement of this study (Gleason score ranged from 6–7, stage ranged from T2b–T2c). Age information was not provided. This information was not taken in to account when collected data was assigned as benign or malignant. Labels correspond only to the presence or absence of disease in the regions of tissue where Raman measurements were acquired.

Sample collection and preparation

Samples were harvested as needle core biopsies (18 gauge spring loaded biopsy gun) and preserved in hypothermosol (Thermo Fisher Scientific, MA, USA). The biopsies were embedded in mounting medium (Tissue-Plus™ O.C.T. Compound, Fisher Scientific, MA, USA), snap frozen in liquid nitrogen and stored at −80° C. Serial (adjacent) tissue sections were obtained for both RS (20 microns thickness) and pathology analysis (H&E staining, 5 micron thickness) by cryosectioning using a rotary cryostat (HM 550; MICROM International GmbH, Walldorf, Germany). Haemotoxylin and eosin staining was performed on frozen tissue sections using the reagents and methodology provided by Abcam (ab245880 H&E stain kit, 2019 protocol).

Spectral acquisition

Needle core biopsies (approximately 0.1 × 0.5 cm) from prostatic adenocarcinoma tumours were sectioned in to 20 micron thick slices using a rotary cryostat (HM 550; MICROM International GmbH, Walldorf, Germany) and placed on magnesium fluoride slides. Spectra were acquired using a Renishaw InVia Raman microscope (Gloucestershire, U.K.) with a 100× dry objective (NA 0.9) (Leica Microsystems, Wetzlar, Germany). All spectra were acquired using a 785 nm diode laser (~30 mW laser power and 0.5 mW μm^{-3} laser power density at sample), 30 seconds acquisition time, and 1 acquisition accumulation per point. The instrument was wavenumber-calibrated using a silicon sample with known peak shifts. For each biopsy slice analysed, 3–5 randomly selected regions were chosen (without prior knowledge of disease/non disease regions) and Raman spectra acquired from a 120 μm^2 area, using 15 micron step size (8 × 8 grid). Spectra were acquired over the range of 450–1800 cm^{-1}. Table 1 shows a summary of spectral parameters used in this study.

Pathology assessment of paired H&E stains

H&E staining was required in order to make a pathological assessment of tissue and assign regions of Raman data as benign or malignant. H&E stained tissue sections were acquired by cutting a 5 micron thick tissue section as a serial section immediately after a 20 micron slice was cut for Raman spectroscopy. This allowed for augmentation of the two tissue sections. During pathology assessment of Raman paired H&E stained biopsies, regions were assigned the category "benign" if no abnormal cells were observed in a given area. As all patients in this study had previously been diagnosed with intermediate risk prostate cancer, it was expected that H&E assessment of the tissue sections with paired Raman analysis would present Gleason scores ranging from 6–8. As such, regions identified as Gleason pattern 3 or pattern 4 were assigned to the category "malignant". The H&E stain produced from flash-frozen OCT-embedded tissue (5 micron thickness) was not of sufficient quality to confidently discriminate between Gleason pattern 3 and Gleason pattern 4 tissue. Therefore, no distinction was made between Gleason pattern and all diseased regions were assigned "malignant". In cases where no pathological assignment could be made confidently, regions were assigned "undetermined" and Raman measurements from those regions were discarded from the dataset.

Table 1 Summary of Raman acquisition and sample preparation parameters

Parameter	Description
Sample type	Needle core prostate biopsy (~0.1 × 0.5 cm)
Section thickness	20 μm (cryostat sectioned)
Substrate	Magnesium fluoride slides
Instrument	Renishaw InVia Raman microscope
Objective	100× dry (NA 0.9)
Excitation wavelength	785 nm diode laser
Laser power	~30 mW (0.5 mW μm^{-3} at sample)
Acquisition time	30 s
Accumulations	1 per spectrum
Calibration	Silicon standard (wavenumber calibration)
Sampling regions	3–5 per biopsy (randomly selected)
Mapping area	120 μm^2 (8 × 8 grid, 15 μm step)
Spectral range	450–1800 cm^{-1}

Spectral processing and analysis

Spectra which contained cosmic rays or saturation were removed prior to spectral processing, as in previous studies.[27] In-house algorithms were used in the estimation and subtraction of spectral background due to fluorescence and to shift the spectra to account for calibration drifts over time (based around the 1003 cm^{-1} phenylalanine peak). Background subtraction was performed using a modified version of the signal removal method described by Schulze *et al.*[36] An initial estimate of the baseline was performed by applying a Savitsky–Golay filter with a window size of 7% of the total range of the data (582 points). This process provides a separation threshold, wherein data above the threshold is deemed signal and data below the threshold is deemed to be noise. Any data above the threshold is replaced with the value of the SG filter BL estimate at that point (*i.e.* the signal is removed). This process is then repeated on the modified data set for 20 iterations (as this number of iterations resulted in no further change of the BL estimate), providing a final estimate of the background spectrum which is then subtracted from the original data. The spectra were then normalised such that the area under the curve was equal to 1. Finally, Savitsky–Golay filtering (window size = 3, order = 1) was used to smooth the data. Group and basis restricted non-negative matrix factorisation (GBR-NMF) was performed on the spectra in order to decompose the data matrix, X, into three lower rank matrices such that,

$$X \approx WAS \quad (1)$$

These three matrices included the chemical bases responsible for variation in the spectra (S), a matrix responsible for scaling the bases (A), and the scores on the bases representing the contribution of each chemical to each spectrum (W). GBR-NMF modelling was carried out using publicly available code for R version ×64 3.6.1, as previously reported.[37] Each of the biochemicals modelled in this study are listed in Table 4 and are assigned a compound class (protein, lipid, carbohydrate, nucleic acid). Biochemicals which are discussed in detail throughout this manuscript are highlighted in grey.

Statistical analysis

Mann–Whitney U-test was applied to assess statistical significance between biochemicals pre- and post-treatment. This test determines if there is a statistically significant difference in median score for each biochemical between two independent groups. This test was chosen as it is non-parametric and makes no assumption that the data is normally distributed. A standard Bonferroni correction was applied as all biochemicals were assessed for statistically significant difference in median score between: benign and malignant tissue, and pre- and post-treatment groups. Statistical significance was displayed as: $p < 0.005$ ***, $p < 0.01$ **, $p < 0.05$ *, n.s. = not significant. This is the case for all statistical significance metrics shown in this manuscript unless otherwise stated.

Results

Raman spectroscopy identifies β-carotene as a marker of malignant prostate tissue

Raman spectroscopy (RS) was employed to derive biochemical profiles from core needle biopsy samples, encompassing both benign and malignant areas, from patients diagnosed with intermediate-grade prostate cancer (PCa). Data were obtained from two biopsies: a pre-treatment biopsy with no prior radiation exposure and a post-treatment biopsy exposed to a single radiation dose of 13.5 Gy. Due to the inherently heterogenous nature of prostate tumour biopsies and loss of data due to poor quality spectra, not every individual yielded both benign and malignant tissue for analysis. Table 2 details the count of Raman spectra obtained from each tissue category (pre-treatment, post-treatment, benign, and malignant) for each individual. Two adjacent tissue sections were collected, one for RS (20 microns) and one for histopathology (5 microns). This facilitated confirmation of the pathology associated with the RS data (*e.g.*, benign, malignant, or undetermined). Tissue which was not classified as either benign or malignant was discarded and not included in further analyses. Typically, 3–5 small tissue areas (approximately 120 μm^2) from each biopsy were subjected to RS analysis, generating roughly 10–60 spectra per region after filtering for cosmic rays and low signal-to-noise ratios. Fig. 1C illustrates an example of RS spectra derived from five different areas within a single biopsy, as shown in Fig. 1A (RS) and B (matching histology). In the RS evaluation of 40 biopsies across 20 patients, distinctive spectral features were identified between benign and malignant tissue regions. Fig. 1C provides an example, where the average spectrum from a benign tissue area is indicated in red, and the average spectra from four separate malignant areas are shown in black. The shadowed spectra illustrate ±1 standard deviation for each region. From Fig. 1C, it is evident that each malignant area exhibited several spectral features not present in the benign tissue spectra, specifically at 957 cm^{-1}, 1157 cm^{-1} and 1524 cm^{-1}. This observation held true for all biopsies analysed in this study.

Table 2 Number of Raman spectra obtained from each individual patient from regions of benign and malignant tissue from both pre-treatment and post-treatment (13.5 fly) biopsies

Patient number	Pre benign	Pre malignant	Post benign	Post malignant
102	687	—	635	—
106	60	70	10	33
115	61	203	220	—
116	188	84	—	104
120	536	—	199	46
121	147	279	117	248
124	—	256	248	117
140	—	45	—	171
157	—	68	47	103
158	85	—	76	—
164	29	—	42	20
178	8	—	24	—
181	68	—	34	—
188	—	52	11	—
196	—	—	37	—
198	—	3	17	16
199	3	—	46	—
200	—	17	6	41
201	70	85	37	89
203	13	2	129	60
Total	1955	1164	1935	1048

In this study, Group and Basis Restricted Non-Negative Matrix Factorisation (GBR-NMF)[27,35] was utilised to enhance the understanding of the biochemical differences contributing to the distinct spectral features between benign and malignant prostate tissue. GBR-NMF is a dimensionality reduction method that yields scores corresponding to the relative abundance of a selected library of biochemicals.[27] Throughout this manuscript, the term biochemical scores refers specifically to these GBR-NMF-derived values. In contrast, spectral features refer to features extracted directly from Raman spectra without deconvolution or dimensionality reduction. Drawing from current research[26] and Raman spectra (Fig. 1E), it was hypothesised that the spectral features at 957 cm^{-1}, 1157 cm^{-1}, and 1524 cm^{-1} observed in malignant tissues could be attributed to carotenoid compounds. The spectral profiles of three carotenoids: carotene, lycopene, and retinol, were incorporated into an existing library of biochemicals for GBR-NMF modelling of Raman spectra collected from prostate tissue. The structure and corresponding Raman spectra of these com-

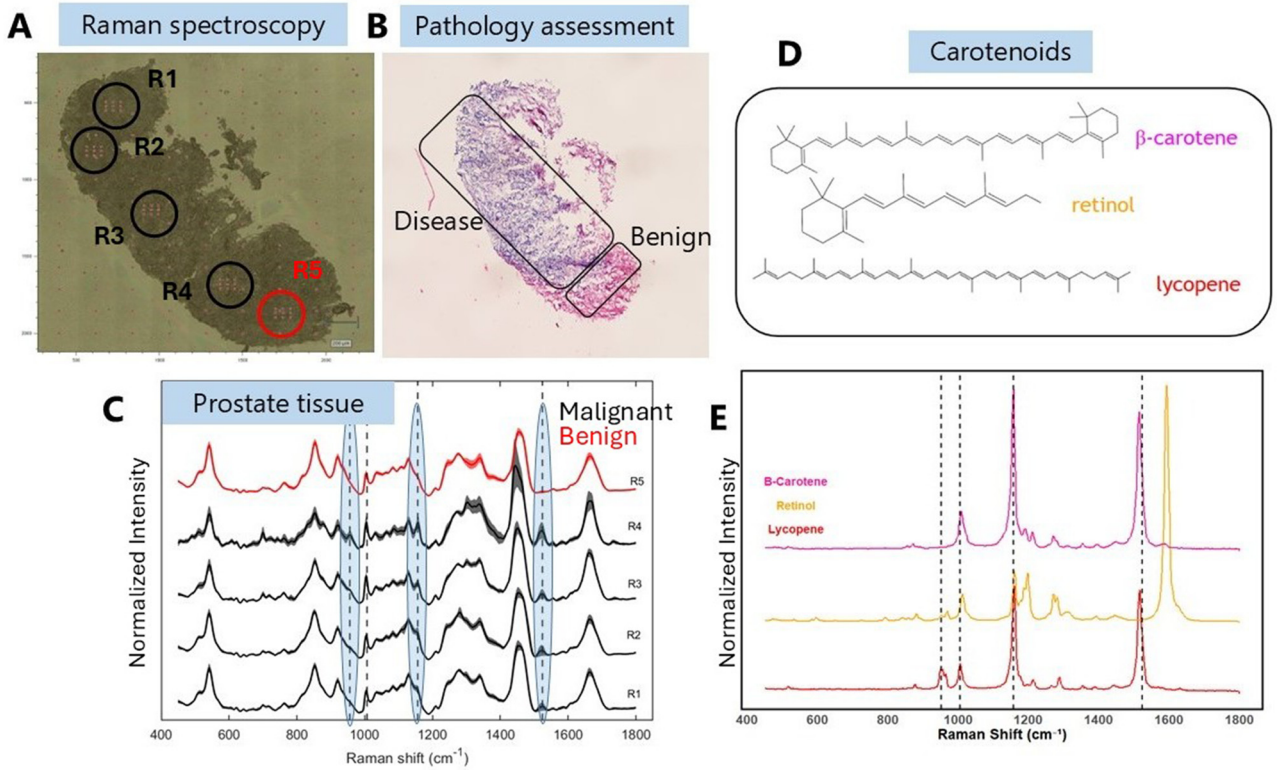

Fig. 1 A. Tissue section used for Raman acquisition. Each circle represents a sampled region (approximately 120 μm^2). Black regions have been matched with pathology analysis (B) and determined to be malignant, red region has been deemed benign. B. Haematoxylin and eosin stain of OCT-embedded 5 micron section of core-needle biopsy from prostate tumour. C. Average Raman spectrum of each region shown in (A, top to bottom = 1–5) showing distinct spectral features at 957 cm^{-1}, 1157 cm^{-1} and 1524 cm^{-1}. Shadow spectrum represents ±1 standard deviation of spectra acquired from each region. D. Structure of carotenoid molecules. E. Raman spectrum of each carotenoid molecule shown in (D) with prominent spectral features identified.

pounds are presented in Fig. 1D and E, respectively. Fig. 1E illustrates that β-carotene and lycopene have a pronounced spectral feature at 1524 cm^{-1}. Moreover, lycopene and retinol revealed less pronounced peaks at 957 cm^{-1}. The spectral features at 1001 cm^{-1} and 1157 cm^{-1} are observed in all three compounds. Tentative band assignments for the three most prominent carotenoid peaks are shown in Table 3. The similarity in the Raman spectra of the carotenoid compounds can be attributed to their analogous chemical structures, as depicted in Fig. 1D. However, this similarity in spectral profile is unlikely to influence the outcomes of GBR-NMF modelling, as indicated by our previous work.[38]

Application of GBR-NMF to RS data collected from the individuals listed in Table 2 revealed distinct biochemical profiles of benign and malignant tissue. Of the 34 biochemicals included in GBR-NMF modelling (including a single unconstrained basis spectrum to allow the model flexibility[27]), 5 biochemicals were significantly differentially expressed (Mann–Whitney *U* Test) between benign and malignant tissue, in the pre-treatment dataset. The biochemicals which were differentially expressed were: palmitic acid, phosphatidylserine, lycopene, retinol and β-carotene. This data is illustrated in Fig. 2. The most distinctive differences in tissue composition were evident in β-carotene and phosphatidylserine (PS) wherein malignant tissue displayed much higher scores for each biochemical. In the post-treatment dataset, β-arotene scores differed significantly between tissue type, however there was no significant difference in PS scores between benign and malignant tissue. Other biochemicals which were differentially expressed between benign and malignant tissue in the post-treatment dataset were: glutathione, histidine and methionine.

Biochemical signatures differ in malignant and benign prostate tissue after a single dose of 13.5 Gy HDR-brachytherapy

Each participant in this study underwent both pre-treatment and post-treatment biopsies, from which Raman spectroscopic data and corresponding histological annotations were obtained. Given that distinct spectral differences and, consequently, significant variations in GBR-NMF scores—were identified between benign and malignant tissue regions, it was hypothesised that the same analytical framework could be applied to assess treatment-induced alterations in biochemical profiles between pre- and post-treatment samples, for both benign and malignant tissues. In HDR-BT research, the dose response relationship of both benign and malignant tissue

Table 3 Assignment of characteristic carotenoid Raman bands with standard mode notation

Raman shift (cm^{-1})	Vibrational description	Associated carotenoids
957	ρCH_3 rocking coupled with C–C skeletal vibrations	Lycopene, β-carotene
1157	ν_2C–C stretching along the conjugated backbone	Lycopene, β-carotene, retinol
1524	ν_1C=C stretching of conjugated polyene chain	Lycopene, β-carotene

Table 4 Classification of biochemicals (ordered as per Fig. 2)

Biochemical	Compound class
Alanine	Amino acid
Arginine	Amino acid
Asparagine	Amino acid
Aspartic acid	Amino acid
Citric acid	Organic acid (TCA cycle metabolite)
Coenzyme A	Metabolic cofactor
Collagen	Structural protein (extracellular matrix)
Cysteine	Amino acid
DNA	Nucleic acid
Glucose	Carbohydrate (monosaccharide)
Glutamic acid	Amino acid
Glutathione	Peptide (tripeptide antioxidant)
Glycerol	Lipid backbone (polyol)
Glycogen	Carbohydrate (polysaccharide)
Histidine	Amino acid
Isoleucine	Amino acid
Lactose	Carbohydrate (disaccharide)
Mannose	Carbohydrate (monosaccharide)
Methionine	Amino acid
Oleic acid	Lipid (monounsaturated fatty acid)
Palmitic acid	Lipid (saturated fatty acid)
Phenylalanine	Amino acid
Phosphatidylcholine	Phospholipid
Phosphatidylserine	Phospholipid
Phosphatidylinositol	Phospholipid
Serine	Amino acid
Stearic acid	Lipid (saturated fatty acid)
Triglycerides	Neutral lipid (triacylglycerol)
Tryptophan	Amino acid
Tyrosine	Amino acid
Valine	Amino acid
Lycopene	Carotenoid (tetraterpene pigment)
Retinol	Carotenoid (vitamin A)
β-Carotene	Carotenoid (provitamin A tetraterpene)

Biochemicals which are discussed in detail in this study are highlighted by grey rows.

remains a poorly understood area. To address the question of how benign and malignant tissue responds to a single dose of 13.5 Gy HDR-brachytherapy (HDR-BT), RS data from each individual were split into four categories: pre-treatment benign, pre-treatment malignant, post-treatment benign and post-treatment malignant. GBR-NMF modelling was applied to the entire data set. The scores for each biochemical were assessed for statistically significant differences between pre-and post-treatment data in the benign and malignant groups separately. This analysis revealed 8 biochemicals which were differentially expressed (Mann Whitney U test, $p < 0.05$) between pre- and post-treatment data in benign tissue: citric acid, collagen, cysteine, DNA, glycerol, palmitic acid, tryptophan and lycopene. Similarly, in malignant tissue, 3 biochemicals were differentially expressed between pre- and post-treatment data: phenylalanine, stearic acid and retinol. Tukey style boxplots depicting the median score for the sub-groups of data for the aforementioned biochemicals are shown in Fig. 3. As some individuals did not yield data from all four categories, the dataset was reduced to include only the individuals which had both pre- and post data for benign tissue (12/20 individuals) and malignant tissue (10/20 individuals). Reduction of the dataset resulted in 4 biochemicals which were significantly different between pre- and post-treatment tissue in the benign dataset (citric acid, glycerol, palmitic acid and lycopene) and 1 biochemical in the malignant dataset (retinol). The difference in score for each biochemical and each individual is shown in Fig. 3 (right) wherein each point represents a single patient. Red points indicate an increase in expression post-treatment whereas blue points indicate a decrease in expression post-treatment. Error bars represent ±1 standard deviation of all RS measurements acquired from an individual.

Discussion

Raman spectroscopy (RS) was used in combination with GBR-NMF modelling[35] to interrogate the biochemical profile of prostate tissue from benign and malignant regions prior to, and two weeks after a single 13.5 Gy dose of HDR-brachytherapy (HDR-BT). Pathology analysis was achieved through serial sectioning of prostate tissue. This allowed for reasonable classification of tissue as benign or malignant and therefore stratification of RS data according to tissue type.

Initial analysis of RS profiles of benign and malignant tissue revealed distinct differences in Raman spectra between the two groups. Most notably, large differences were observed at 957 cm^{-1}, 1157 cm^{-1} and 1524 cm^{-1} as shown in Fig. 1C, wherein all peaks showed greater intensity in malignant areas of tissue. Analysis of relevant literature and inclusion of three carotenoid compounds in the GBR-NMF spectral library (Fig. 1D & E) revealed β-carotene and PS to differ significantly between pre-treatment benign and malignant prostate tissue (Fig. 2). In recent years, there has been significant interest in the role of phospholipids in both diagnosis and prognosis of prostate cancer. Phospholipids, such as phosphatidylcholine, phosphatidylethanolamine, phosphatidylinositol, PS, and sphingomyelin play a critical role in the plasma membrane of both healthy and malignant cells. PS has gained particular attention due to its presence on the exterior membrane of prostate cancer cells, a feature not observed in healthy cells. This unique feature of PCa allows for selective targeting of PCa cells, whilst sparing healthy cells, thus making PS a candidate for selective therapies.[39] As altered PS expression is a hallmark of PCa, it is therefore plausible that RS combined with GBR-NMF identified PS as one of two distinguishing biochemicals between malignant and normal tissue. Interestingly, PS

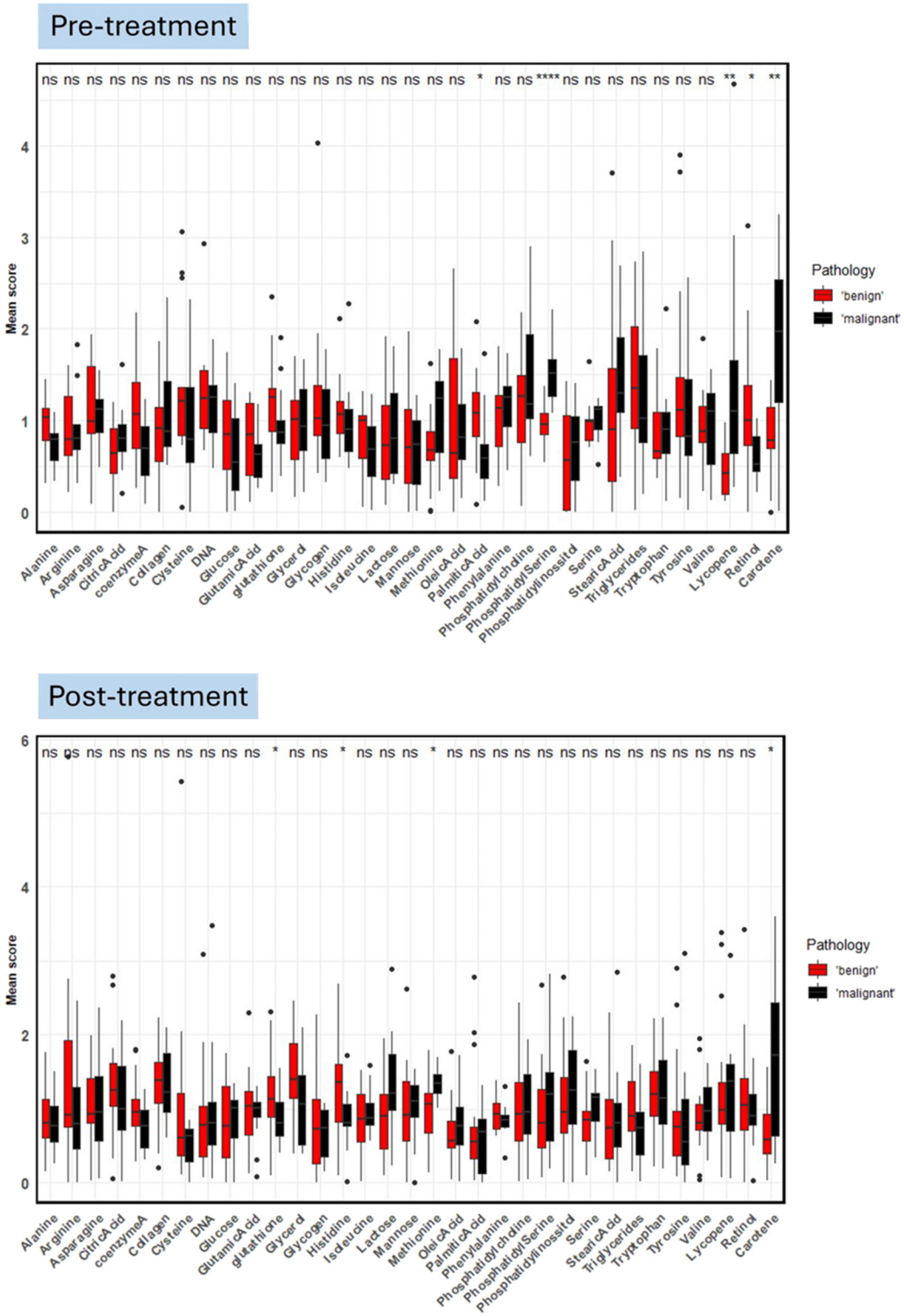

Fig. 2 Tukey style boxplot displaying the scores for 33 biochemicals obtained from RS analysis of benign (red) and malignant (black) tissue from all individuals with available data. Asterisks represent *p*-values ($p < 0.005$ ***, $p < 0.01$ **, $p < 0.05$ *, n.s. = not significant) for pre-treatment prostate tissue (top) and post-treatment (13.5 fly) prostate tissue (bottom). Mean scores are relative flBR-NMF scores and are comparable within biochemicals.

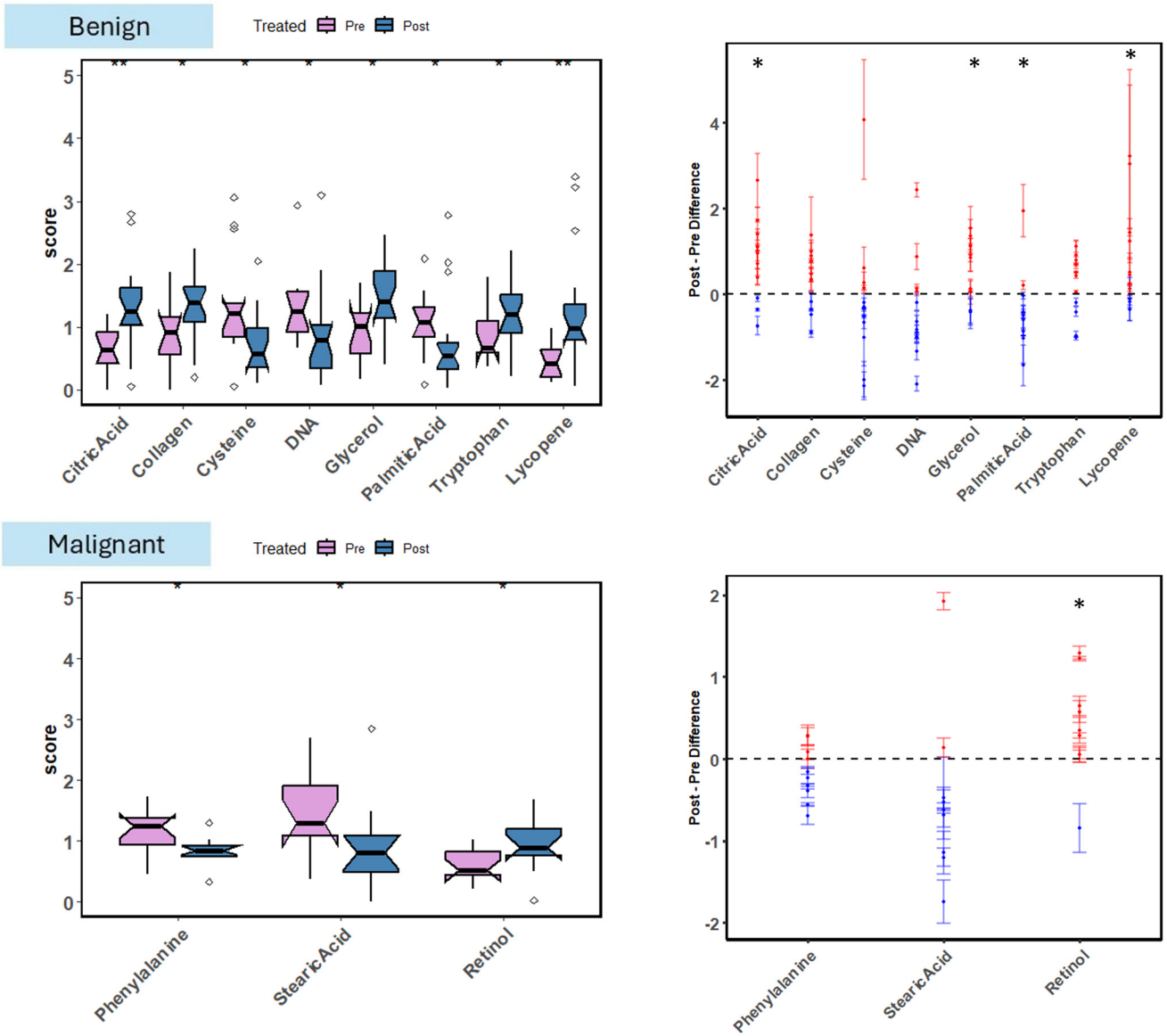

Fig. 3 Left: Tukey style boxplots depicting the median score for pre-treatment biopsies (purple) and post-treatment biopsies (blue) for benign (top) and malignant (bottom) datasets. Biochemicals shown are those which were statistically significantly different between pre- and post-treatment data (Mann–Whitney *U* test). Right: The difference in score for each individual. Multiple spectra were acquired for each individual biopsy from the same patient, therefore the difference score here is the median post-treatment score minus the median pre-treatment score, for both benign and malignant tissue types. Each point represents a single patient. Red points indicate an increase in expression post-treatment and blue points indicate a decrease in expression post-treatment. Error bars represent ±1 standard deviation of all RS measurements acquired from an individual. Asterisks indicate biochemicals which remained statistically significant when the dataset was reduced to contain only individuals with both pre- and post data for each tissue type.

did not differ between benign and malignant tissue in the post-treatment data subset (Fig. 2). This could be due to initiation of cell death within malignant regions after HDR-BT, and therefore the presence of fewer functioning malignant cells capable of altered PS expression. This is a particularly interesting difference between the pre- and post-treatment samples as the individuals involved in this study have received only a single fraction of 13.5 Gy. This observation could therefore provide insight to the involvement of PS as a lipid involved in early radiation response. Whilst not a novel candidate as a marker of PCa, this result is well documented in current literature and therefore highlights the potential of RS as a reliable method of tissue characterisation in oncology applications. Most investigations which endeavour to produce a metabolic profile of PCa focus exclusively on serum analysis.[40] Whilst serum is obtained more readily than excised tissue, metabolic and biochemical profiling of PCa tissue could aid in better understanding of the tumour environment and identification of potential therapeutic targets.

In contrast to PS, β-carotene, which was identified as a marker of PCa by RS, has not been well researched in terms of specific association with PCa as a diagnostic or prognostic biomarker. A 2020 study by Correia *et al.*[41] showed that patients with PSA levels above 4.0 ng mL^{-1} had greater carotenoid content in their blood serum as opposed to patients with a normal PSA range of <4.0 ng mL^{-1}. In this study, we identified β-carotene alongside PS as the two most significant differentially expressed biochemicals (out of a total library of 34 biochemicals) between normal prostate tissue and malignant prostate tissue, in a cohort of 20 patients (Fig. 2). Carotenoids are antioxidants obtained from many edible plants and fruits. Among them, β-carotene, lycopene and retinol (vitamin A) are some of the most widely studied in terms of their association with risk of developing cancer. Early research in this area focused on dietary intake of carotenoids and the associated increased or decreased risk of developing certain cancers,[42] such as lung,[43] breast,[44,45] and prostate cancer.[46–49] However, more recent research has focused on carotenoids as therapeutic agents or prognostic markers. For example, Morasso *et al.*[50] identified decreased carotenoid expression in dried plasma as a marker of colorectal cancer. Many studies have claimed lycopene to play a role in reduced tumour proliferation and favourable prognosis[51] due to inhibition of PCa cell growth[52] and altered metabolism.[53] Similarly, serum retinol levels have been positively associated with increased risk of prostate cancer in multiple studies.[54–56] Most research in this area has focused on serum concentration of carotenoids and therefore the link between carotenoids as a marker of malignant prostate tissue and the role carotenoids play in the tumour environment remains unclear. A major finding of this investigation was that both β-carotene and PS expression was significantly higher in malignant tissue than in benign prostate tissue. This was observed in both the Raman spectrum (increased peak intensity at 954, 1157 and 1524 cm^{-1}) and the GBR-NMF modelling of the data, which provides greater specificity over spectral interpretation. Whilst greater PS content in malignant prostate tissue may be unsurprising, β-carotene has not yet been established as a marker of malignancy in PCa and warrants further investigation as a potential therapeutic target. Based on existing literature,[57] it can be hypothesised that β-carotene is involved in the altered lipid metabolism observed in prostate cancer due to its strong lipophilic nature and dependence on lipid transport and storage systems such as lipoproteins and cellular membranes. Prostate tumours are known to undergo extensive lipid metabolic reprogramming, including increased lipid uptake, *de novo* lipogenesis, and membrane remodelling, which may create conditions that favour the accumulation or altered distribution of β-carotene within malignant tissue. Within this framework, observed differences in β-carotene levels between benign and cancerous prostate tissue may reflect downstream consequences of tumour-associated lipid dysregulation and oxidative stress.

Higher methionine content in malignant regions aligns with current research on increased uptake of methionine in PCa cell lines when compared with normal cells.[58] Conversely, lower levels of glutathione and histidine in PCa is in contradiction to many other studies which have created a metabolic profile of PCa, however it is worth noting that most of these studies focused on serum analysis.[40,59,60] Generally, research involving the role of lycopene and lycopene metabolism in PCa has been conflicting and there is insufficient evidence to determine whether increased lycopene in pre-treatment malignant tissue compared with pre-treatment benign tissue should be expected.[11,61,62]

In addition to creating a biochemical and metabolic profile of benign and malignant prostate tissue, we also assessed how each tissue type responded to a single dose of 13.5 Gy RT. This dose was delivered to the prostate as the first fraction of a 27 Gy/2 fraction HDR-brachytherapy treatment regimen and post-treatment biopsies were collected approximately 2 weeks after the first fraction. The aim of this analysis was to determine how the biochemical composition of both benign and malignant tissue changed as a result of irradiation with a single dose of 13.5 Gy, as this question remains largely unanswered in HDR-brachytherapy research.[63,64]

Analysis of RS data pre- and post-treatment revealed distinct biochemical changes of both benign and malignant tissue. Benign prostate tissue revealed significant differences in a much greater number of biochemicals (citric acid, collagen, cysteine, DNA, glycerol, palmitic acid, tryptophan and lycopene) than for the malignant subtype. However, when only patients with both pre- and post benign data were considered (12/20 patients) the number of significant biochemicals reduced to four (citric acid, glycerol, palmitic acid and lycopene). The scores for each biochemical pre- and post-treatment is shown as a boxplot in Fig. 3. Each patient contributes a single point within the boxplot. Additionally, the change in each biochemical score between pre- and post-treatment biopsies, per tissue type is shown for each individual in the right-hand panel of Fig. 3. Only individuals with both pre-and post data are shown, red points indicate an increase in score and blue points indicate a decrease in score after RT. Considering only the reduced patient group (12 individuals), nine patients displayed an increase in lycopene and glycerol in post-treatment benign tissue, one individual displayed a decrease in average lycopene and glycerol score, however consideration of the standard deviation of all RS measurements collected from that individual results in error margins which could indicate a slight increase in both lycopene and glycerol score post-treatment. Two individuals exhibited a slight decrease in lycopene and glycerol score post-treatment. This trend was similar for citric acid, wherein 3/12 individuals exhibited decreased citric acid in post-treatment benign tissue. Palmitic acid was generally found to decrease in post-treatment benign tissue, again with the exception of 2 individuals. Increased citric acid in benign prostate tissue as a result of radiation exposure could be due to oxidative stress and effects on the citrate-orientated metabolism of normal prostate tissue.[65] We speculate that glycerol and palmitic acid involvement may be due to apoptosis and/or altered lipid signalling and phospholipid remodelling to promote radiation resistance.[66,67] The role of lycopene in

benign prostate tissue response is unclear, however increased lycopene could provide protective effects against oxidative stress and DNA damage.[68]

Analysis of malignant prostate tissue initially revealed phenylalanine, stearic acid and retinol as biochemicals with significant changes in expression after radiation. However, reduction of the dataset to include only those patients with both pre- and post-treatment data (10/20 patients) reduced this list to only retinol. From Fig. 3 it can be seen that with the exception of one individual (patient 106), all other individuals exhibited increased levels of retinol post radiation. Studies investigating the link between retinol and PCa prognosis are limited and have produced mixed results. For example, a 2011 study by Mondul *et al.*[69] found higher serum retinol to be associated with elevated risk of developing prostate cancer, whilst Schenk *et al.*[70] found higher levels of serum retinol to be correlated with decreased risk of developing aggressive prostate cancer. A 2016 study by Li *et al.*[71] found retinol inhibited the growth of PC-3 prostate cancer cells. Research evaluating retinol involvement in radiation therapy is extremely limited. The interaction between retinol pathways and radiation-induced cellular damage remains an area for future research. Further studies are needed to elucidate the effects of radiation on retinol levels within prostate cancer tissues and to understand the implications for cancer progression and treatment outcomes.

Whilst we have shown here the potential of RS to characterise PCa tissue and assess the radiation response of different tissue types, there are limitations to this study which should be addressed. Firstly, no Gleason grading was provided during pathology analysis. This is a limitation of OCT-embedded histology which is required for RS analysis of adjacent sections of tissue. We speculate that tissue composition may vary dependent on Gleason grade and that this could alter the biochemical profile of the tissue. However, every patient included in this study was deemed Gleason grade 6 or 7 *e.g.* intermediate risk disease (based on FFPE H&E analysis of a separate diagnostic biopsy) and therefore we would not expect large discrepancies between tissue composition of these individuals based on Gleason grade alone. Secondly, due to limited sampling of tissue with RS due to time limitations with air-exposed tissue as well as loss of data in the cleaning/processing stage, not every individual yielded data from both tissue types and/or treatment status, thus limiting the number of patients with a full compliment of data available for analysis.

Conclusions

Complexity and heterogeneity of tissue composition in PCa is still poorly understood and we have shown here the capabilities of a RS based approach to profile and characterise PCa on a biochemical level. As such, corroborating current research on altered lipid metabolism and increased expression of PS in PCa, as well as identification of β-carotene as a novel tissue marker for PCa. Additionally, characterisation of both benign and malignant tissue in terms of radiation response to a single dose of HDR-brachytherapy has revealed distinct biochemical changes in benign and malignant tissue and revealed carotenoids as a potential therapeutic target in the treatment of PCa. The prevalence of carotenoids (β-carotene, lycopene and retinol) as biochemicals which differed significantly in expression between the different tissue types assessed in this study merits further investigation. Future studies could endeavour to investigate the relationship between carotenoid expression and treatment outcomes in PCa patients, specifically how this relates to treatment outcomes of HDR-brachytherapy.

Author contributions

K. M., A. J. and J. C. conceived the experiment(s), K. M. conducted the experiment(s), K. M., M. W., S. P., A. F. and R. A. analysed the spectroscopy data. B. N. T. provided the pathology assessment of biopsy cores. All authors provided insight to analysis and reviewed the manuscript.

Conflicts of interest

The authors declare no competing interests.

Data availability

Data can be found at https://osf.io/84gb9.

Supplementary information (SI) is available. See DOI: https://doi.org/10.1039/d6an00128a.

Acknowledgements

This work is supported by grant funding from the Natrual Sciences and Engineering Research Council of Canada (grant no. RGPIN-2020-07232 and RGPIN-2020-04646) and the Candian Institute of Health Research (PJT 162279).

References

1 Canadian Cancer Society, Prostate Cancer, https://cancer.ca/en/about-us/prostate-cancer, 2025, accessed: 2024-01-30.
2 S. C. Kamran and A. V. D'Amico, *Hematol. Oncol. Clin. North Am.*, 2020, **34**, 45–69.
3 I. S. Williams, A. McVey, S. Perera, J. S. O'Brien, L. Kostos, K. Chen, S. Siva, A. A. Azad, D. G. Murphy, V. Kasivisvanathan, N. Lawrentschuk and M. Frydenberg, *Med. J. Aust.*, 2022, **217**, 424–433.
4 S. C. Kamran and A. L. Zietman, *BJU Int.*, 2021, **128**, 398–407.
5 J. Crook, M. Marbán and D. Batchelar, *Semin. Radiat. Oncol.*, 2020, **30**, 49–60.

6 H. E. Barker, J. T. Paget, A. A. Khan and K. J. Harrington, *Nat. Rev. Cancer*, 2015, **15**, 409–425.
7 A. M. Monjazeb, K. A. Schalper, F. Villarroel-Espindola, A. Nguyen, S. L. Shiao and K. Young, *Semin. Radiat. Oncol.*, 2020, **30**, 145–157.
8 M. E. Takashima, T. J. Berg and Z. S. Morris, *Semin. Radiat. Oncol.*, 2024, **34**, 262–271.
9 S. Liu, W. Wang, S. Hu, B. Jia, B. Tuo, H. Sun, Q. Wang, Y. Liu and Z. Sun, *Cell Death Dis.*, 2023, **14**, 679.
10 W. Boulefour, E. Rowinski, S. Louati, S. Sotton, A. S. Wozny, P. Moreno-Acosta, B. Mery, C. Rodriguez-Lafrasse and N. Magne, *Med. Sci. Monit.*, 2021, **27**, e934116.
11 E. J. Moon, K. Petersson and M. M. Olcina, *Int. J. Radiat. Biol.*, 2022, **98**, 439–451.
12 C. Beckers, M. Pruschy and I. Vetrugno, *Semin. Cancer Biol.*, 2024, **98**, 19–30.
13 J. L. Rowles and J. W. Erdman, *Biochim. Biophys. Acta, Mol. Cell Biol. Lipids*, 2020, **1865**, 158613.
14 L. Koklesova, A. Liskova, M. Samec, K. Zhai, M. Abotaleb, M. Ashrafizadeh, A. Brockmueller, M. Shakibaei, K. Biringer, O. Bugos, M. Najafi, O. Golubnitschaja, D. Büsselberg and P. Kubatka, *Biomolecules*, 2020, **10**, 1–26.
15 Y. Hussain, Abdullah, K. F. Alsharif, M. Aschner, A. Theyab, F. Khan, L. Saso and H. Khan, *Nutrients*, 2022, **14**, 1949.
16 R. Niranjana, R. Gayathri, S. N. Mol, T. Sugawara, T. Hirata, K. Miyashita and P. Ganesan, *J. Funct. Foods*, 2015, **18**, 968–985.
17 X. Gong, J. R. Smith, H. M. Swanson and L. P. Rubin, *Molecules*, 2018, **23**, 905.
18 J. Sui, J. Guo, D. Pan, Y. Wang, Y. Xu, G. Sun and H. Xia, *Foods*, 2024, **13**, 1321.
19 L. W. Lu, Y. Gao, S. Y. Quek, M. Foster, C. T. Eason, M. Liu, M. Wang, J. H. Chen and F. Chen, *Biomed. Pharmacother.*, 2022, **154**, 113625.
20 L. N. Jiang, Y. B. Liu and B. H. Li, *Asian J. Androl.*, 2019, **21**, 80–85.
21 K. Zu, L. Mucci, B. A. Rosner, S. K. Clinton, M. Loda, M. J. Stampfer and E. Giovannucci, *J. Natl. Cancer Inst.*, 2014, **106**, djt430.
22 M. Mirahmadi, S. Azimi-Hashemi, E. Saburi, H. Kamali, M. Pishbin and F. Hadizadeh, *Biomed. Pharmacother.*, 2020, **129**, 110459.
23 X. Zhang, Q. Wang, N. Barber and X. Chen, *Chin. Med. J.*, 2010, **123**, 2231–2236.
24 N. E. Moran, B. Alexander, S. Garg, N. Marchant and N. A. Hason, *J. Nutr.*, 2024, **154**, 3639–3651.
25 C. H. Pernar, E. M. Ebot, K. M. Wilson and L. A. Mucci, *Cold Spring Harbor Perspect. Med.*, 2018, **8**, a030361.
26 A. C. S. Talari, Z. Movasaghi, S. Rehman and I. U. Rehman, *Appl. Spectrosc. Rev.*, 2015, **50**, 46–111.
27 K. Milligan, X. Deng, P. Shreeves, R. Ali-Adeeb, Q. Matthews, A. Brolo, J. J. Lum, J. L. Andrews and A. Jirasek, *Sci. Rep.*, 2021, **11**, 3853.
28 X. Deng, K. Milligan, R. Ali-Adeeb, P. Shreeves, A. Brolo, J. J. Lum, J. L. Andrews and A. Jirasek, *Appl. Spectrosc.*, 2022, **76**, 462–474.
29 M. J. Baker and K. Faulds, *Chem. Soc. Rev.*, 2016, **45**, 1792–1793.
30 J. C. Greig, W. J. Tipping, D. Graham, K. Faulds and G. W. Gould, *Analyst*, 2024, **149**, 4789–4810.
31 S. Laing, L. E. Jamieson, K. Faulds and D. Graham, *Nat. Rev. Chem.*, 2017, **1**, 0060.
32 A. M. Batista, L. Foiani, M. Champeau and H. Martinho, *J. Raman Spectrosc.*, 2022, **53**, 1848–1860.
33 K. Milligan, X. Deng, R. Ali-Adeeb, P. Shreeves, S. Punch, N. Costie, J. M. Crook, A. G. Brolo, J. J. Lum, J. L. Andrews, *et al.*, *Sci. Rep.*, 2022, **12**, 15104.
34 M. Wiebe, K. Milligan, J. Brewer, A. M. Fuentes, R. Ali-Adeeb, G. Brolo, J. J. Lum, J. L. Andrews, C. Haston and A. Jirasek, *Analyst*, 2024, **149**, 2864–2876.
35 P. Shreeves, J. L. Andrews, X. Deng, R. Ali-Adeeb and A. Jirasek, *Stat. Biosci.*, 2023, **15**, 608–632.
36 G. Schulze, A. Jirasek, M. M. L. Yu, A. Lim, R. F. B. Turner and M. W. Blades, *Appl. Spectrosc.*, 2005, **59**, 545–574.
37 J. Andrews and P. Shreeves, *Group and Basis Restricted Non-Negative Matrix Factorization*, https://github.com/its-likeli-jeff/GBRNMF, 2024, accessed: 2025-01-01.
38 K. Milligan, K. Scarrott, J. L. Andrews, A. G. Brolo, J. J. Lum and A. Jirasek, *Appl. Spectrosc.*, 2023, **77**, 698–709.
39 S. Preetam, A. Pandey, R. Mishra, G. Mohapatra, P. Rath, S. Malik, S. Rustagi, A. Dash and S. K. Samal, *Mater. Adv.*, 2024, **5**, 8384–8403.
40 A. P. S. Pita, M. M. Escudero, E. Jiménez-Charris and H. A. García-Perdomo, *J. Cancer Res. Clin. Oncol.*, 2025, **151**, 29.
41 N. A. Correia, L. T. Batista, R. J. Nascimento, M. C. Cangussú, P. J. Crugeira, L. G. Soares, L. Silveira Jr and A. L. Pinheiro, *J. Photochem. Photobiol., B*, 2020, **204**, 111801.
42 N. I. Krinsky and E. J. Johnson, *Mol. Aspects Med.*, 2005, **26**, 459–516.
43 L. Gallicchio, K. Boyd, G. Matanoski, X. Tao, L. Chen, T. K. Lam, M. Shiels, E. Hammond, K. A. Robinson, L. E. Caulfield, J. G. Herman, E. Guallar and A. J. Alberg, *Am. J. Clin. Nutr.*, 2008, **88**, 372–383.
44 M. K. Dehnavi, S. Ebrahimpour-Koujan, K. Lotfi and L. Azad-bakht, *Adv. Nutr.*, 2024, **15**, 100135.
45 L. I. Mignone, E. Giovannucci, P. A. Newcomb, L. Titus-Ernstoff, A. Trentham-Dietz, J. M. Hampton, W. C. Willett and K. M. Egan, *Int. J. Cancer*, 2009, **124**, 2929–2937.
46 T. J. Key, P. N. Appleby, R. C. Travis, D. Albanes, A. J. Alberg, *et al.*, *Am. J. Clin. Nutr.*, 2015, **102**, 1142–1157.
47 D. V. Hoang, N. M. Pham, A. H. Lee, D. N. Tran and C. W. Binns, *Nutrients*, 2018, **10**, 70.
48 J. L. Watters, M. H. Gail, S. J. Weinstein, J. Virtamo and D. Albanes, *Cancer Res.*, 2009, **69**, 3833–3841.
49 E. Giovannucci, A. Ascherio, E. B. Rimm, M. J. Stampfer, G. A. Colditz and W. C. Willett, *J. Natl. Cancer Inst.*, 1995, **87**, 1767–1776.
50 C. Morasso, E. Daveri, A. Bonizzi, M. Truffi, F. Colombo, P. Danelli, S. Albasini, L. Rivoltini, S. Mazzucchelli, L. Sorrentino and F. Corsi, *MedComm*, 2024, **5**, e774.

51 J. Dulińska-Litewka, Y. Sharoni, P. Hałubiec, A. Łazarczyk, O. Szafrański, J. A. McCubrey, B. Gąsiorkiewicz, P. Laidler and T. Bohn, *Antioxidants*, 2021, **10**, 585.
52 M. Kelkel, M. Schumacher and M. Diederich, *Free Radical Res.*, 2011, **45**, 925–940.
53 L. Tang, T. Jin, X. Zeng and J.-S. Wang, *J. Nutr.*, 2005, **135**, 287–290.
54 S. H. Nash, C. Till, X. Song, M. S. Lucia, H. L. Parnes, I. M. Thompson, S. M. Lippman, E. A. Platz and J. Schenk, *Cancer Epidemiol., Biomarkers Prev.*, 2015, **24**, 1507–1515.
55 D. Cao, Y. Meng, S. Li, J. Xin, S. Ben, Y. Cheng, M. Wang, L. Hua and G. Cheng, *Cancer Med.*, 2020, **9**, 9462–9470.
56 W. Q. Loh, X. Yin, R. Kishida, S. E. Chia, C. N. Ong and W. J. Seow, *Nutrients*, 2023, **15**, 2677.
57 J. Dulińska-Litewka, Y. Sharoni, P. Hałubiec, A. Łazarczyk, O. Szafrański, J. A. McCubrey, B. Gąsiorkiewicz, P. Laidler and T. Bohn, *Antioxidants*, 2021, **10**, 585.
58 V. Strmiska, P. Michalek, T. Eckschlager, M. Stiborova, V. Adam, S. Krizkova and Z. Heger, *Biochim. Biophys. Acta, Rev. Cancer*, 2019, **1871**, 248–258.
59 U. Peters, M. F. Leitzmann, N. Chatterjee, Y. Wang, D. Albanes, E. P. Gelmann, M. D. Friesen, E. Riboli and R. B. Hayes, *Cancer Epidemiol., Biomarkers Prev.*, 2007, **16**, 962–968.
60 G. E. Valenti, B. Tasso, N. Traverso, C. Domenicotti and Marengo, *Redox Exp. Med.*, 2023, **2023**, e220023.
61 X. Gong, R. Marisiddaiah, S. Zaripheh, D. Wiener and L. P. Rubin, *Mol. Cancer Res.*, 2016, **14**, 966–975.
62 M. B. Sporn and K. T. Liby, *Cancer Prev. Res.*, 2013, **6**, 384–386.
63 A. J. Stewart, C. Chargari, A. Chyrek, F. Eckert, J. L. Guinot, T. P. Hellebust, P. Hoskin, C. Kirisits, B. Pieters, F. A. Siebert, L. Tagliaferri, K. Tanderup, D. Todor, P. Wojcieszek and J. M. Hannoun-Levi, *Clin. Transl. Radiat. Oncol.*, 2025, **50**, 100885.
64 C. Chargari, E. V. Limbergen, U. Mahantshetty, E. Deutsch and C. Haie-Méder, *Cancer Radiother.*, 2018, **22**, 312–318.
65 F. Ahmad, M. K. Cherukuri and P. L. Choyke, *Br. J. Cancer*, 2021, **125**, 1185–1196.
66 D. An, D. Zhai, C. Wan and K. Yang, *Clin. Transl. Oncol.*, 2023, **25**, 2332–2349.
67 L. P. Fernández, M. G. de Cedrón and A. R. de Molina, *Front. Oncol.*, 2020, **10**, 577420.
68 V. S. Dhillon, P. Deo and M. Fenech, *Cancers*, 2023, **15**, 979.
69 A. M. Mondul, J. L. Watters, S. Männistö, S. J. Weinstein, K. Snyder, J. Virtamo and D. Albanes, *Am. J. Epidemiol.*, 2011, **173**, 813–821.
70 J. M. Schenk, E. Riboli, N. Chatterjee, M. F. Leitzmann, J. Ahn, D. Albanes, D. J. Reding, Y. Wang, M. D. Friesen, R. B. Hayes and U. Peters, *Cancer Epidemiol., Biomarkers Prev.*, 2009, **18**, 1227–1231.
71 C. Li, M. Imai, T. Matsuura, S. Hasegawa, M. Yamasaki and N. Takahashi, *Biol. Pharm. Bull.*, 2016, **39**, 636–640.